Vision as a Compensatory Mechanism for Disturbance Rejection in Upwind Flight

Michael B. Reiser[1], J. Sean Humbert[2], Mary J. Dunlop, Domitilla Del Vecchio,
Richard M. Murray, and Michael H. Dickinson

Abstract—Recent experimental results demonstrate that flies posses a robust tendency to orient towards the frontally-centered focus of the visual motion field that typically occurs during upwind flight. In this paper we present a closed loop flight model, with a control algorithm based on feedback of the location of the visual focus of contraction, which is affected by changes in wind direction. The feasibility of visually guided upwind orientation is demonstrated with a model derived from current understanding of the biomechanics and sensorimotor computation of insects. The matched filter approach used to model the visual system computations compares extremely well with open-loop experimental data.

I. INTRODUCTION

Flies have served as a model system for neurobiological studies of vision and flight [1], [2], and therefore detailed information is immediately available for biomimetic applications. In this paper we investigate the possibility of using the fly's vision system as the means of counteracting the effect of wind disturbances during upwind flight. To establish the feasibility of visually-guided upwind orientation we have constructed a detailed closed-loop flight simulation, making use of current research in insect biomechanics and neurophysiology.

There have been many efforts in the past to apply mathematical models to the flight behavior of insects. Much of the earlier work modeled the tracking behavior of flies [3], [4], [5]. The most significant of these is the effort by Reichardt and Poggio [6] to rigourously model the orientation behavior of flies with a closed loop model. All of these earlier models lumped the entire sensory-input (visual) to motor-output (torque produced by the wings) pathway of the fly in a single black box. In recent years studies have focused on the visual processing of insects, revealing simple algorithms for collision avoidance based on estimating optic flow, a local measurement of intensity motion across the retina [7], [8]. This has inspired several robotic implementations of insect-based control systems [9], [10], [11], [12].

The work we present here is very much in the tradition of these earlier efforts to model tracking behavior in insects. We have used the improved understanding of the aerodynamics of insect flight [13], the force production of realistic wing kinematics [14], and the higher-level processing in the insect visual system, to 'shrink' the black boxes in earlier models. We seek to demonstrate that through a faithful model of the fly's behavior, it is possible to provide some context within which controlled behavioral assays can

[1] mreiser@caltech.edu, [2] jshumber@cds.caltech.edu
All authors are in the Division of Engineering and Applied Science, California Institute of Technology, Pasadena, CA 91125.

be interpreted. The results presented here demonstrate the feasibility of visually-guided upwind orientation, and have yielded strong agreement with experimental results.
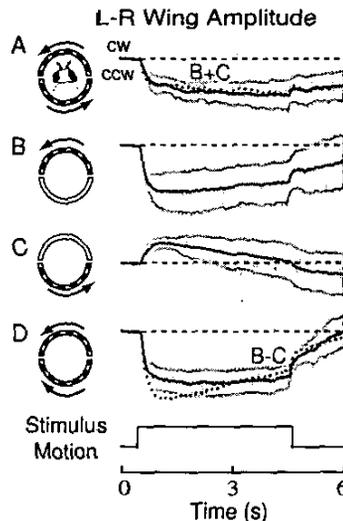
L-R Wing Amplitude

Fig. 1. Open loop visuo-motor reflexes in *Drosophila*. These data has been replotted from Tammero *et al.* [15]. The quantity plotted on the vertical axis is the difference between the right and left wing beat amplitudes measured by an optical sensor. Each trace represents the mean ± S.D. (shaded area), from 10 flies.

Fig. 1 shows the results of recent work [15]. In these experiments large-field motion stimuli were presented in open loop to tethered flies. Fig. 1 A–D shows the averaged turning response of the flies measured from an optical sensor that records wing activity. Fig. 1A corresponds to the classic optomotor response [16], in which the fly responds to coherent full field rotatory motion by turning to minimize retinal slip. The plots in B and C show the mean response of the fly to front and rear field rotatory motion. The response in A is shown to be the sum of the responses in B and C (red line). However, the response in C, clearly contradicts the predictions of the optomotor response, since the attempted turn is not in the direction that would minimize the rotatory stimuli. The response in D shows that the strongest response is obtained when the fly attempts to orient towards a contracting focus of the motion stimulus. This shows that the fly can detect the location of the visual focus of contraction (or is doing something functionally equivalent). The focus of contraction (expansion) is the point of no motion in a velocity field induced by pure translation, that all motion vectors point towards (away from). These data suggest that a control algorithm based on feedback of the movement of the visual focus of contraction could be used to detect wind direction, since upwind flight induces a frontally-centered focus of the visual motion field.
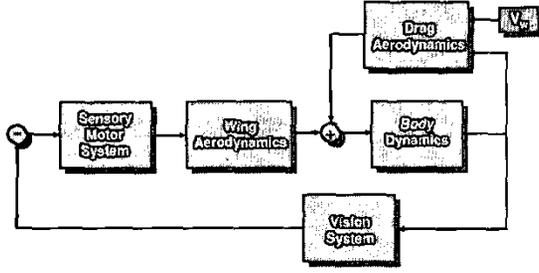
Fig. 2. Closed loop model used for study of upwind flight. V_w is the wind disturbance, a vector quantity.

II. CLOSED LOOP MODEL OF UPWIND FLIGHT

A closed loop representation of the fly's control system (Fig. 2) is divided into several blocks including body dynamics and body aerodynamics (plant), the wing aerodynamics (actuator), the vision system (sensor) and the sensorimotor system (controller). The function of the body dynamics block is to take as inputs the forces and torques from the wing and body aerodynamics blocks and produce the resultant translational and rotational motion of the insect body. In the body aerodynamics block the inputs are the wind velocity magnitude and direction, the body velocity and the body rotational position, and the outputs are the resultant aerodynamic forces on the body. The left and right wing kinematics are the inputs to the wing aerodynamics block, which outputs the resultant aerodynamic forces on the body due to wing motion. The function of the vision system block is to take as inputs the inertial translational and rotational velocity and output an estimate of the visual focus of contraction location (error). The loop is closed through the sensorimotor block, which generates parameterized values for controlled wing kinematics from the estimate of the visual focus of contraction location.

III. BODY DYNAMICS

We close the loop in our model around a single axis of rotation. Therefore, we have restricted the dynamics of the insect body to planar translatory motion along a single axis of rotary motion (Fig. 3A). In our simulation we ignore out-of-plane forces, however the forces generated from our wing kinematic model are of the order required to balance

the weight of the insect. The translational position, r, and rotational position, ϕ, are defined by $r = x\hat{e}_x + y\hat{e}_y$ and $\phi = \phi\hat{e}_z$, where $\hat{e}_z = \hat{e}_x \times \hat{e}_y$. The map from inertial coordinates, r, to body fixed coordinates, r_b, is given by:

$$r_b = \begin{pmatrix} \cos\phi & \sin\phi \\ -\sin\phi & \cos\phi \end{pmatrix} r.$$

We assume the the insect has mass, m, rotational inertia about the ϕ axis, J, and experiences applied force $F = F_{x_b}(t)\ \hat{e}_{x_b} + F_{y_b}(t)\ \hat{e}_{y_b}$, and torque $T = T_\phi(t)\ \hat{e}_{z_b}$. The equations of motion under these assumptions are given by Newton's second law:

$$\begin{bmatrix} m\ddot{x} \\ m\ddot{y} \\ J\ddot{\phi} \end{bmatrix} = \begin{bmatrix} F_{x_b}\cos\phi - F_{y_b}\sin\phi \\ F_{x_b}\sin\phi + F_{y_b}\cos\phi \\ T_\phi \end{bmatrix}.$$

The resultant applied force F and torque T are due to the aerodynamic forces on the wings and body (Section V). Wing motion generates unsteady lift and drag, which is well-approximated with a quasi-steady model. The body aerodynamic forces result from the relative velocity of the body with respect to the free stream (wind), and the drag associated with rotation of the body about the z axis:

$$\begin{aligned} F_{x_b}(t) &= F_{Aero,x_b}(t) + F_{Wind,x_b}(t) \\ F_{y_b}(t) &= F_{Aero,y_b}(t) + F_{Wind,y_b}(t) \\ T_\phi(t) &= T_{Aero}(t) - C\dot{\phi}(t). \end{aligned}$$

Fry and coworkers (2003) measured the rotational inertia, J, and damping, C, about the morphological yaw axis (normal to the insect body). As we intend to use the functional axis of rotation (Fig. 3A) for this simulation, we assume that the differences in these constants about the two axes are negligible.

In order to characterize the aerodynamic forces on the insect body during flight, we analyzed data from experiments performed with Robofly, a dynamically-scaled physical model of a flapping insect. An insect-shaped body was subjected to a range of forward velocities in an oil tank at various angles of attack, with the resultant forces recorded and reduced to parallel and normal force coefficients (Fig. 3C). The size of the body was scaled so that the Reynolds
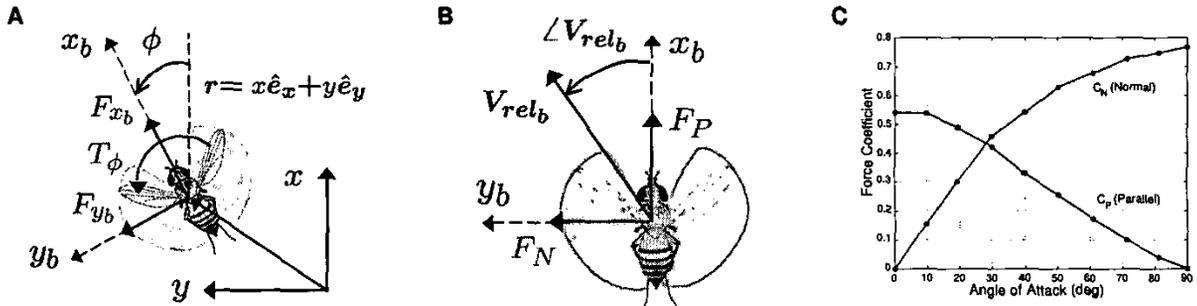

Fig. 3. (A) Insect coordinate frames showing body forces and torques; (B) Force directions acting on the insect body; (C) Force coefficients for parallel and normal aerodynamic forces.
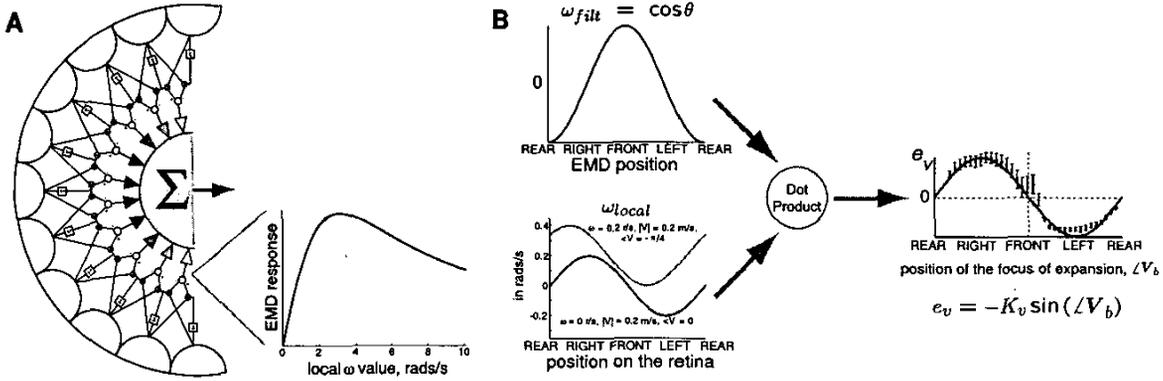
312

Fig. 4. Two representations of the visual system modeling. Fig. (A) shows a schematic diagram of the retina and the motion processing and matched filter circuitry. A typical EMD response is also shown. Fig. (B) shows the operations of the matched filter on the velocity field vector. The filter is minimally responsive to the upwind flight profile of local velocities. The filtering process is a projection (dot product). The data superimposed on the filter result is excerpted from Tammero *et al.* [15], showing the open loop turning response of *Drosophila* to the location of the focus of expansion. This simple model of open-loop visual response agrees well with data from tethered *Drosophila*.

number ($Re \approx 200$) matches what a typical insect sees during nominal flight ($0.1 - 0.3 \, m/s$).

The relative velocity of the insect with respect to the air (Fig. 3B) is determined by the wind direction and magnitude, the body velocity, and the orientation (all specified in inertial coordinates): $V_{rel} = V_{wind} - \dot{r}$. Since the aerodynamic forces will be computed in the body frame, we need the relative velocity in body coordinates:

$$\begin{pmatrix} V_{rel,x_b} \\ V_{rel,y_b} \end{pmatrix} = \begin{pmatrix} \cos\phi & \sin\phi \\ -\sin\phi & \cos\phi \end{pmatrix} \begin{pmatrix} V_{rel,x} \\ V_{rel,y} \end{pmatrix}.$$

The magnitude and phase in body coordinates is then

$$|V_{rel_b}| = \sqrt{V_{rel,x_b}^2 + V_{rel,y_b}^2}$$
$$\angle V_{rel_b} = \text{atan2}(V_{rel,y_b}, V_{rel,x_b}).$$

Now we can compute the resultant aerodynamic forces:

$$F_{Wind,x_b} = \frac{1}{2}\rho A \, |V_{rel_b}|^2 \, C_P(\angle V_{rel_b})$$
$$F_{Wind,y_b} = \frac{1}{2}\rho A \, |V_{rel_b}|^2 \, C_N(\angle V_{rel_b}),$$

where ρ is the density of air, A is the projected cross-sectional area of the insect, $|V_{rel_b}|$ and $\angle V_{rel_b}$ are the magnitude and phase of the relative velocity in body coordinates, and C_N, C_P are the normal and parallel force coefficients that have been reduced from the experimental force data.

IV. VISION SYSTEM

Each compound eye of the *Drosophila melanogaster* consists of approximately 700 units, called ommatidia, arranged in a hexagonal array. Each ommatidium samples a round patch of about 5° of the visual world. The 1400 ommatidia can sample roughly 85% of the visual space [17]. To account for the experimentally observed optomotor response in insects, Hassenstein and Reichardt proposed a model of visual motion detection based on arrays of spatiotemporal correlation elements [18]. A local motion detector must

theoretically consist of at least two inputs passing through asymmetrical channels and combined via a nonlinear element [19]. Two of these half-detectors are combined (with mirror-symmetry) to form a directionally-selective Elementary Motion Detector (EMD). In the Hassenstein-Reichardt model, a temporal delay provides the asymmetry and multiplication is the nonlinear interaction. In the simulation presented, the fly's retina is modeled as a circular array of 90 receptor/EMD units, with $4°$ spacing between receptors. In general, the response of an EMD is dependent on the visual system structure, i.e. the time delay and the spacing of the receptors in the retina, and also on properties of the visual input, such as image contrast and spatial frequency content. Fig. 4A shows an EMD array, as well as a typical response curve for an EMD corresponding to the environment statistics used in the presented simulations. It is important to note the distinction between the velocity field, a purely geometric object, and the optic flow field, which is the estimate of the velocity field experienced by a moving fly, as computed by the EMDs.

Krapp and Hengstenberg [20] show that the tangential neurons of the lobula plate in the blowfly, *Calliphora*, show strong preference to certain directions of local motion. Individual tangential cells receive inputs from many EMDs and output signals that appear tuned to estimate a particular feature of the optic flow field that the fly would experience by self-motion during flight [21], [20]. This observation has given rise to the idea that certain cells function as 'matched filters' to patterns of optic flow that could directly drive the flight control muscles. Applying these ideas to our simulated planar world, the optic flow field is a vector spanning the field of view. For flight oriented in the direction of the wind, there cannot be a sideslip component to the local velocities measured by the EMDs. Flies exhibit a preference for orienting towards the focus of contraction of the velocity field, which means they can only orient upwind if they are flying slower than the wind.
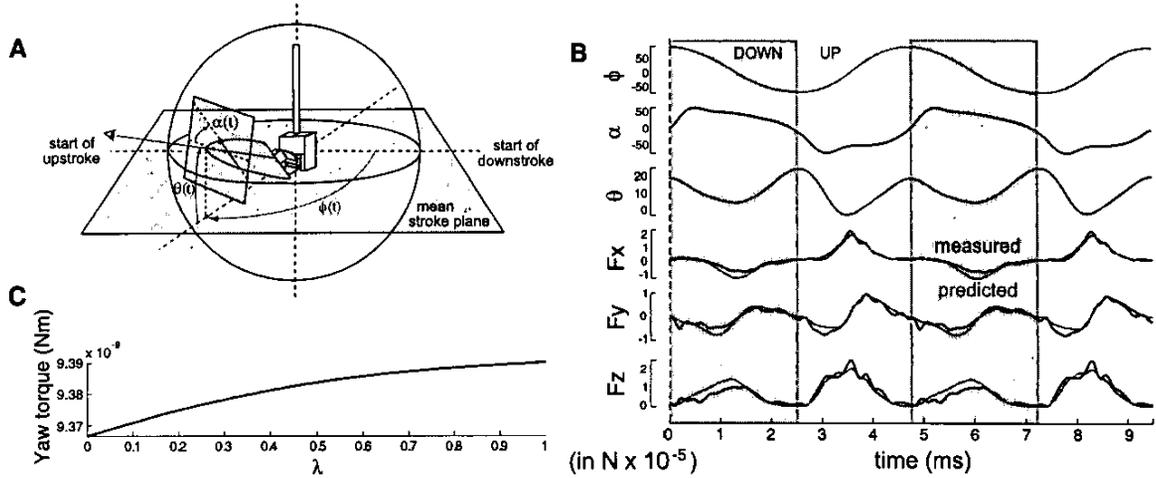
313

Fig. 5. The sensorimotor control system interpolates between captured wing kinematics to generate yaw torques. (A) Wing angle parameterizations for the robotic apparatus used to measure aerodynamic forces. (B) Two wing strokes captured from *Drosophila* in free flight and the corresponding flight forces measured on the robot and computed via a quasi-steady model. (C) Torque about the fly's yaw axis produced by one wing as a function of the control parameter.

This suggests a simple strategy for visual wind detection—fly slowly and seek out foci of contraction. We designed a filter that is minimally responsive to the desired profile of local velocities (the equilibrium condition). Because these responses are (roughly) sinusoids, the reasonable filter is simply the profile itself but phase shifted by 90°, and the filtering process is the dot product of the two curves. This interpretation of matched filters agrees with some of the Lobula Plate Tangential Cells, which give cosine-like response to stimulation in various directions (with a peak in the so-called locally-preferred direction). An example of the filtering process and some typical velocity field vectors are shown in Fig. 4B. Since the EMD array produces an estimate of the velocity field, it is instructive to analyze the filtering process on the velocity field (true optic flow):

$$\omega_{local} = \omega_o - \frac{|V_b|}{R} \sin(\theta - \angle V_b),$$

where ω_o is the instantaneous rotation, V_b is the instantaneous absolute velocity in body coordinates, θ is the angular coordinate in the body frame, and R is an arbitrary fixed distance to the environment. The matched filter is $\omega_{filt} = \cos\theta$, and the filtering operation is a dot product,

$$
\begin{aligned}
e_v &= \langle \omega_{local}(\theta), \omega_{filt}(\theta) \rangle \\
&= \frac{1}{2\pi} \int_0^{2\pi} \omega_{local} \cdot \omega_{filt} \, d\theta \\
&= -K_v \sin(\angle V_b),
\end{aligned}
$$

where K_v is the gain used in the visual system. As we can see in Fig. 4B, this open loop result agrees well with the experimental data from Tammero *et al.* [15]. In our simulation we use the EMD array's estimate of the velocity

fields, which does not alter the fundamental shape of this response curve, but is not amenable to simple analysis.

V. WING AERODYNAMICS AND SENSORIMOTOR CONTROL

The flight forces generated by the simulated fly's wings are implemented as a quasi-steady, semi-empirical model (details of this model are given in Sane and Dickinson [14]). In general, the instantaneous force produced by a wing is the sum of several effects: translation, rotation, added mass, and other unsteady effects. All of these forces act normal to the wing, which rotates, translates, and deviates continuously throughout a single wing stroke (the parameterization of the wing kinematics is shown in Fig. 5A). The translational force is the dominant term, accounting for roughly 90% of the force generated by the wing. In our simulations, we only use the translational component of the aerodynamic forces. To further simplify matters, the fly is assumed to hover, thus operating at an advance ratio of zero. Although not strictly valid, the hovering model provides a reasonable force estimate for a fly moving slowly (advance ratios under 0.3). Fig. 5B shows the performance of this simplified model in comparison to the forces measured when the same wing kinematics are run on the robotic model. The torque produced by each wing about the fly's yaw axis is determined directly from the force vector predicted by the aerodynamic model. The right and left wings often take on distinct wing kinematics. The net force and torque generated by the wings combines the contributions from right and left wings appropriately: $F_{Aero,x_b} = F_{x,left} + F_{x,right}$; $F_{Aero,y_b} = F_{y,left} - F_{y,right}$; $T_{Aero} = T_{yaw,left} - T_{yaw,right}$.

Wing kinematics were selected from an existing database of wing stroke patterns that correspond to actual insect kinematics (the collection of these data is detailed in Fry *et al.* [13]). We choose wing kinematics using two selection
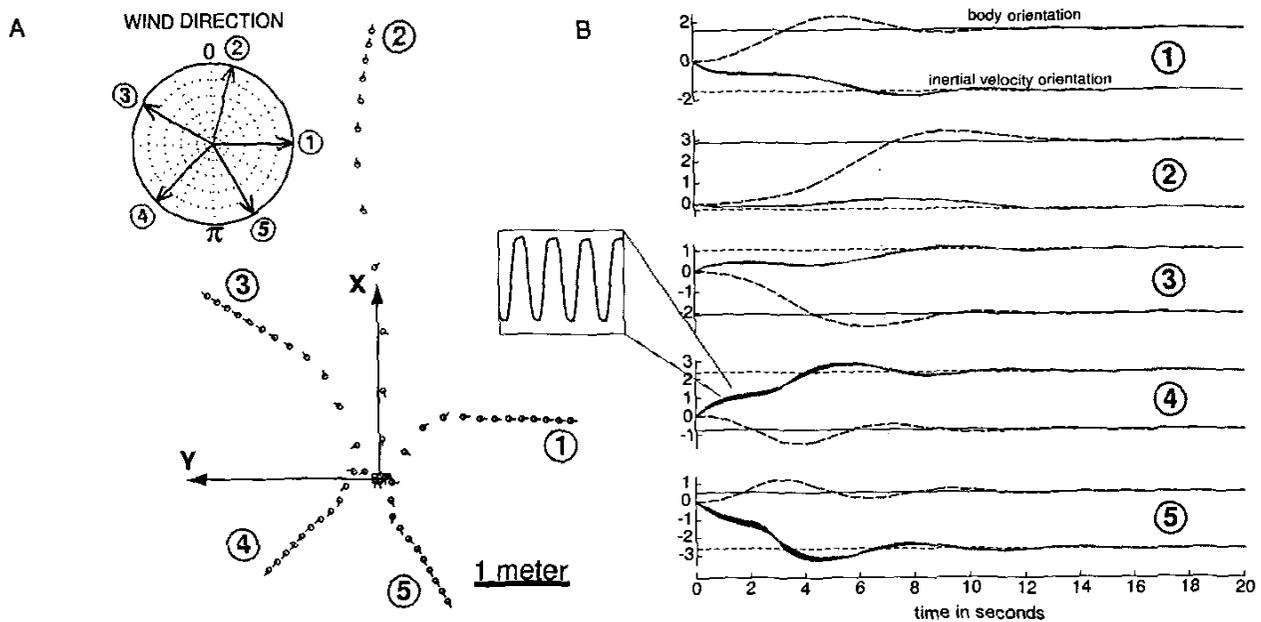
Fig. 6. Two equivalent representations of responses to step changes in wind direction are shown: (A) simulated 20 second flight trajectories, with fly positions plotted every 1.5 seconds. All trajectories start at the origin, and the wind direction is shown in the compass. (B) Step responses in wind direction, showing zero steady-state error. The high frequency oscillations shown correspond to the subtle perturbations on the fly's instantaneous velocity induced by the wing stroke cycle. All measurements are in radians.

criteria: the force in the x direction should result in forward flight not exceeding velocities of 30 cm/s (advance ratio of approximately 0.3) and yaw torques must correspond to realistic angular rotations. Since the model uses only the relatively slow visual system, it is necessary to limit torque about the yaw axis, effectively limiting the rate of angular rotation the insect experiences. The yaw torque requirement stipulates that the difference in torque between the right and left wing should be on the order of 10^{-11} Nm. Two sets of wing kinematics were selected that met the criteria discussed above, one corresponding to low torque kinematics and the second to kinematics generating higher torque. We define a parameter, λ, to span the range of wing stroke kinematics between the low and high torque patterns. The parameter λ ranges smoothly between 0 and 1, defining a linear weighting between the two endpoint kinematics. Fig. 5C shows the torque about the fly's yaw axis produced by one wing as a function of λ. We have found that linearly interpolating between two sets of kinematics gives a smooth transition between the forces produced by these endpoint kinematics. In our simulation we refer to the sensorimotor block as the control system that couples the sensory information from the visual system to the flight muscles. This system takes the error from the visual system as an input and generates the control values for each wing: $\lambda_R = 1 - k|e_v|I_{(0,\infty)}(e_v)$, and $\lambda_L = 1 - k|e_v|I_{(-\infty,0]}(e_v)$, where k is the control system gain, and $I_{(-\infty,0]}(e_v)$ is an indicator function whose value is 1 when $e_v \in (-\infty, 0]$, and 0 otherwise. Furthermore, e_v is restricted to the range $[-1, 1]$ to ensure that λ_R and λ_L are in the range $[0, 1]$.

VI. RESULTS

The stated goal of the project is to modulate upwind flight, and so our controller sets the torque about the fly's yaw axis. To test the ability of the closed loop system to orient the fly in the upwind direction, we presented 'step inputs' to the control system, where the fly was given an initial velocity and orientation and the wind was set at a fixed magnitude and direction. In the experiments presented, the fly's initial orientation is set in the positive x (forward) direction, with some small (0.1 m/s) velocity in the same direction. The wind magnitude is set at 0.4 m/s, which is always faster than anything the fly could achieve. Five different wind directions are then introduced.

Two equivalent ways of displaying the results are shown in Fig. 6. In each plot of Fig. 6B, the dashed horizontal line shows the wind direction set point; the solid horizontal line shows the desired body orientation angle for upwind flight; the solid trace corresponds to the orientation of the inertial reference frame velocity; the dashed trace corresponds to the body orientation angle. The numbered markers on the right side of each response plot correspond to the numbered trajectories and wind directions in Fig. 6A. It is clear from both representations of the step responses that the tracking works, in the sense that the steady state error is driven to zero, resulting in upwind orientation.

From the step response and frequency response data (Fig. 7) it is clear that the closed loop system is stable. Stability of this system corresponds to orientation upwind, evidenced by the zero steady state error in the step response plots. Cast as a tracking problem, the tracking error is the amount of
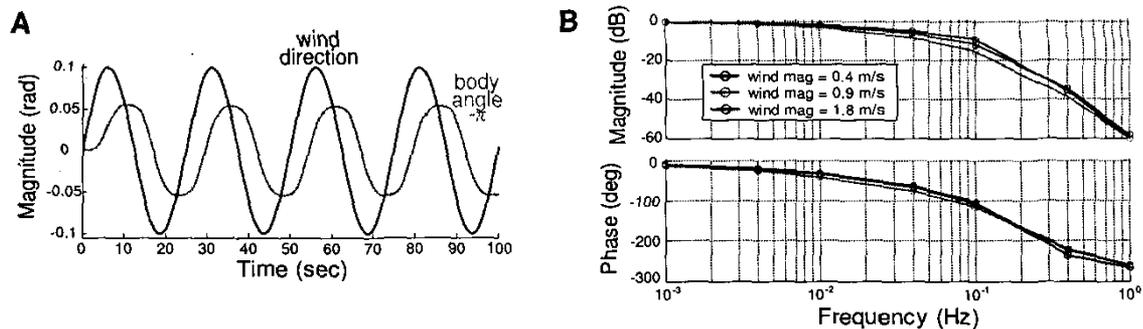
Fig. 7. Closed loop frequency response. (A) Time domain response to a small signal disturbance of fixed frequency. (B) Small signal frequency response to disturbances in wind heading for several wind magnitudes.

sideslip the fly experiences, which is the difference between the inertial velocity orientation and the orientation of the fly's body (these are the two step responses plotted in Fig. 6). For (backwards) upwind flight this difference should be π, which is achieved at steady state, so the tracking error is zero. Interpreting the frequency response data shown in Fig. 7 in terms of tracking the mean wind direction, we can see the system is insensitive to disturbances, except at very low (less than 0.01 Hz) frequencies. Furthermore, the frequency response is not significantly affected by changing wind speeds.

VII. CONCLUSIONS

In this project we have investigated the use of the fly's vision system as a sensory modality to counteract the effect of wind disturbances during upwind flight. A closed loop insect flight simulation was constructed based on realistic models of the physics and biology, demonstrating the feasibility of visually guided upwind orientation.

Closed loop simulations show stable upwind orientation behavior over the range of behaviorally-relevant wind speeds (0.4 to 1.2 m/s) and sensitivity only to very low frequency disturbances (0.01 Hz). The resulting open loop response of the visual sensory system, based on a matched filter approach used to model the computations performed in insects, agrees extremely well with open loop experimental data gathered from real animals [15].

In future work we expect to extend this simulation to three dimensions and six degrees of freedom, and investigate vision algorithms that take advantage of global optic flow cues. Also of immediate interest is the velocity control problem associated with transition from backwards to forward flight in the upwind direction.

REFERENCES

[1] M. Egelhaaf and R. Kern, "Vision in flying insects," Curr. Opin. Neurobiol., vol. 12, no. 6, pp. 699–706, 2002.

[2] M. A. Frye and M. H. Dickinson, "Fly flight: a model for the neural control of complex behavior," Neuron, vol. 32, no. 3, pp. 385–388, 2001.

[3] M. Land and T. Collett, "Chasing behavious of houseflies Fannia canicularis. A. description and analysis," J. comp. Physiol. A., vol. 89, no. 4, pp. 331–357, 1974.

[4] R. Virsik and W. Reichardt, "Detection and tracking of moving objects by the fly Musca domestica," Biol. Cybern., vol. 23, no. 2, pp. 83–98, 1976.

[5] T. S. Collett and M. F. Land, "Visual control of flight behavior in hoverfly, Syritta pipiens." J. Comp. Physiol., vol. 99, pp. 1–66, 1975.

[6] W. Reichardt and T. Poggio, "Visual control of orientation behavior in fly. Part 1. a quantitative analysis," Quartetly Reviews of Biophysics, vol. 9, no. 3, pp. 311–375, 1976.

[7] M. V. Srinivasan, M. Poteser, and K. Kral, "Motion detection in insect orientation and navigation," Vis. Res., vol. 39, no. 16, pp. 2749–2766, 1999.

[8] L. F. Tammero and M. H. Dickinson, "The influence of visual landscape on the free flight behavior of the fruit fly Drosophila melanogaster," J. Exp. Biol., vol. 205, no. 3, pp. 327–343, 2002.

[9] N. Franceschini, J. M. Pichon, and C. Blanes, "From insect vision to robot vision," Phil. Trans. R. Soc. Lond. B, vol. 337, pp. 283–294, 1992.

[10] M. V. Srinivasan, J. S. Chahl, M. G. Nagle, and S. W. Zhang, "Embodying natural vision into machines," in From Living Eyes to Seeing Machines, M. Srinivasan and S. Venkatesh, Eds. U.K.: Oxford University Press, 1997, pp. 249–265.

[11] K. Weber, S. Venkatesh, and M. V. Srinivasan, "Insect inspired behaviours for the autonomous control of mobile robots," in From Living Eyes to Seeing Machines, M. Srinivasan and S. Venkatesh, Eds. U.K.: Oxford University Press, 1997, pp. 226–248.

[12] M. Reiser and M. Dickinson, "A test bed for insect-inspired robotic control," Philos. T. Roy. Soc. A, vol. 361, no. 1811, pp. 2267–2285, 2003.

[13] S. Fry, R. Sayaman, and M. Dickinson, "The aerodynamics of free-flight maneuvers in Drosophila," Science, vol. 300, no. 5618, pp. 495–498, 2003.

[14] S. Sane and M. Dickinson, "The aerodynamic effects of wing rotation and a revised quasi-steady model of flapping flight," J. Exp. Biol., vol. 205, no. 8, pp. 1087–1096, 2002.

[15] L. F. Tammero, M. A. Frye, and M. H. Dickinson, "Spatial organization of visuomotor reflexes in Drosophila," J. Exp. Biol., vol. 207, no. 1, pp. 113–122, 2004.

[16] K. G. Götz, "Flight control in Drosophila by visual perception of motion," Kybernetik, vol. 9, pp. 159–182, 1968.

[17] M. Heisenberg and R. Wolf, Vision in Drosophila. Berlin: Springer Verlag, 1984.

[18] W. Reichardt, "Autocorrelation, a principle for relative movement discrimination by the central nervous system," in Sensory Communication, W. Rosenblith, Ed. New York: MIT Press, 1961, pp. 303–317.

[19] A. Borst and M. Egelhaaf, "Principles of visual motion detection," Trends Neurosci., vol. 12, pp. 297–306, 1989.

[20] H. G. Krapp and R. Hengstenberg, "Estimation of self-motion by optic flow processing in single visual interneurons," Nature, vol. 384, pp. 463–466, 1996.

[21] K. Hausen, "The lobula-complex of the fly: structure, function and significance in visual behaviour," in Photoreception and vision in invertebrates, M. Ali, Ed. New York: Plenum Press, 1984, pp. 523–559.